Journal of Archaeological Science: Reports 66 (2025) 105278

Contents lists available at ScienceDirect

Journal of Archaeological Science: Reports

journal homepage: www.elsevier.com/locate/jasrep

# Using archaeomagnetism to unravel the occupational history of a medieval site: Cañada Real (Burgos, Northern Spain)

Eva Vernet [a,*], Ángel Carrancho [b], Manuel Calvo-Rathert [a], Yuhji Yamamoto [c], Susana E. Jorge [d], María F. Bógalo [a], Ángel Palomino [e]

[a] Departamento de Física, EPS, Universidad de Burgos, Av. Cantabria, s/n, 09006 Burgos, Spain
[b] Área de Prehistoria, Departamento de Historia, Geografía y Comunicación, Universidad de Burgos 09001 Burgos, Spain
[c] Marine Core Research Institute, Kochi University, Kochi 783-8502, Japan
[d] Área de Geodinámica Interna, Facultad de Humanidades y Educación, Universidad de Burgos 09001 Burgos, Spain
[e] Área de Arqueología y Proyectos Culturales, Patrimonio Global, 47009 Valladolid, Spain

ARTICLE INFO

*Keywords:*
Archaeomagnetism
Archaeomagnetic dating
Archaeointensity
Medieval period
Thermoremanence

ABSTRACT

Different attempts to date the archaeological site of Cañada Real (Northern Spain) with radiocarbon yielded contrasting results, ranging from the Bronze Age to medieval times. During the archaeological interventions carried out there, a well-preserved burned surface was discovered. The burned sediments of this surface offered the opportunity to conduct full-vector archaeomagnetic dating to elucidate the age of the studied site. For determination of an archaeomagnetic intensity, two different methods (Thellier-Coe and Tsunakawa-Shaw) were applied to test their suitability and compare their reproducibility. Raman spectroscopy and rock magnetism revealed that the main magnetization carrier is magnetite, with varying concentrations of hematite and goethite. A good correlation is observed between high Q*n* ratio values (typically > 6) and strongly magnetic as well as stable orthogonal demagnetization diagrams of the natural remanent magnetization. The full-vector was recovered with a mean direction of Declination = 17.7°, Inclination = 54.0°, $\alpha_{95}$ = 3.2°, $k$ = 309.2 and a mean intensity of 38.1 ± 9.0 μT. Comparison to the SCHA.DIF.4 k geomagnetic field model yielded a single dating interval of 995–1125 CE at 95 % confidence level. This result accurately dates one of the phases of abandonment of the site and coincides with some historically documented Muslim *razzias*, demonstrating the usefulness of the archaeomagnetic technique to reconstruct the occupational history of archaeological sites with burned remains.

## 1. Introduction

A fundamental issue in any archaeological study is chronology. Determining a precise age to reconstruct the history and use of a site, the duration of human occupations in the past and when a site was abandoned are key topics in archaeology. Nevertheless, this task is not always straightforward. On the one hand, relative dating methods (e.g., stratigraphic seriation, artifact typology, biochronology, etc.) provide valuable chronological frameworks, but they do not yield precise age estimates. On the other hand, absolute methods can provide one or more age intervals with their associated temporal uncertainties, which vary depending on the method used, the material analyzed, and its age (e.g.: Walker, 2005). Among the latter are the luminescence dating and its variants (e.g.: optical stimulated luminescence or OSL, thermoluminescence or TL), electron spin resonance (ESR), uranium–thorium (U/Th) or radiocarbon ($^{14}$C), just to name a few. Of all of them, and as far as dating materials younger than *ca.* 50,000 yr BP are concerned, $^{14}$C is probably the best known and most widely used method in archaeology. However, even extensively used and long-established methods like $^{14}$C exhibit some limitations (e.g.: Hervé and Lanos, 2018), though this happens with any other dating method. Ideally, different methods should be applied and compared to check their reproducibility and to analyse the underlying causes of its suitability.

One of such methods is the archaeomagnetic dating technique. It is based on the ability of the ferromagnetic minerals –iron-containing minerals, mainly iron oxides, hydroxides, or some sulphides- contained in the burned materials to record the Earth's magnetic field (EMF) at the time of the last burning and subsequent cooling, as a natural remanent magnetization (NRM). If the heating exceeds the Curie temperature ($T_C$) of the ferromagnetic minerals present (e.g.: 580 °C for magnetite or

* Corresponding author.
*E-mail address:* evernet@ubu.es (E. Vernet).

https://doi.org/10.1016/j.jasrep.2025.105278
Received 24 January 2025; Received in revised form 16 June 2025; Accepted 16 June 2025
Available online 20 June 2025

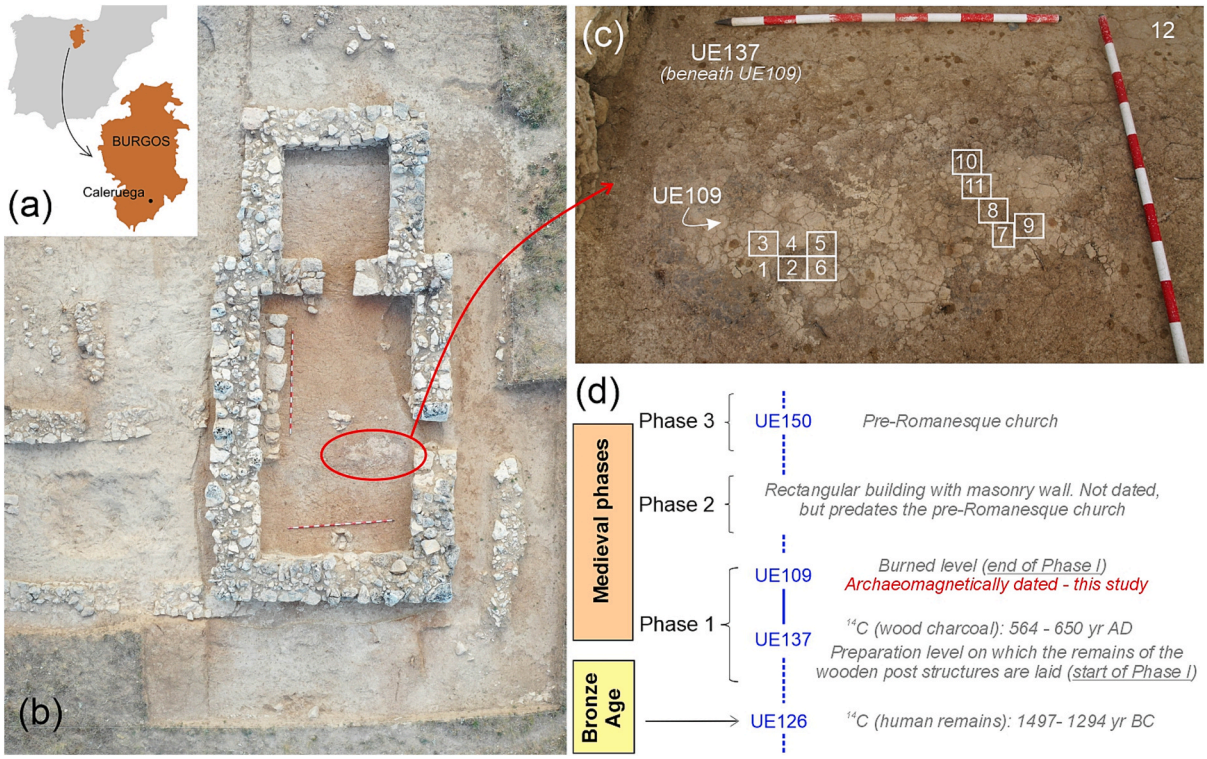


**Fig. 1.** (a) Location of Cañada Real site in Caleruega (Burgos, North Spain). (b) Photogrammetry of the archaeological site, the studied burnt surface is circled. (c) Detailed picture of the burnt surface with the location of the samples taken indicated. (d) Stratigraphic scheme indicating the phases of activity, stratigraphic units (UE), a brief description of what each one represents and available dates.

675 °C for hematite; Dunlop and Özdemir, 1997), the material is susceptible to record a full thermoremanent magnetization or TRM (e.g. Tauxe, 2010; Batt 2023). This TRM is a snapshot and usually stable record of the direction and intensity of the EMF. Heated below the Curie temperature, the material can acquire a partial thermoremanence or p-TRM that can also be an efficient record of the EMF in the past. The EMF varies with time consistently on a regional scale both in direction (magnetic declination and inclination) and intensity, and this is a process known as *secular variation* (SV). Previous efforts in the archaeomagnetic study of archaeological combustion structures carrying a TRM and independently well-dated, have allowed to establish regional SV curves and global geomagnetic field models for the last millennia (e.g.: Di Chiara and Pavón-Carrasco, 2022; García-Ruiz et al. 2022; Kovacheva et al. 2014; Pavón-Carrasco et al. 2021; Molina-Cardín et al. 2018; Schanner et al. 2022; Tema and Lanos 2021; Gomez-Paccard et al., 2006). These curves and geomagnetic field models have been already utilized for dating and constitute a powerful chronometric tool for archaeology (e.g. García-Redondo et al. 2019, 2020). Recently, a unique application of archaeomagnetism to temporarily dissect Middle Paleolithic human occupations has been published (Herrejón-Lagunilla et al. 2024). While in the Balkans geomagnetic reference curves have been used as a dating tool for more ancient archaeological sites (e.g. Jordanova et al. 2004; Aidona and Kondopoulou 2012), in Western Europe this technique has mostly been used to date burned archaeological materials from the last IV-V millennia (Carrancho et al. 2022).

In the archaeological site of Cañada Real (Northern Spain) studied here, different and apparently inconsistent radiocarbon dates had been previously obtained. They vary over a wide range from the Bronze Age (2nd millennium BC) to the Middle Ages (*ca.* XII century AD). The site has been interpreted as the remains of an early medieval church although with different phases of occupation (Palomino and Crespo, 2022). The discovery of a burned sediment surface inside the church remains offered a good opportunity to perform a full-vector archaeomagnetic dating in order to clarify the age of last burning of one of the phases of occupation and to check its consistency with the radiocarbon dates.

This study aims: (i) to date by means of a full-vector archaeomagnetic study the last heating and abandonment of one of the phases of occupation of the site; and (ii) to discuss the obtained archaeomagnetic dating and its coherence with the available radiocarbon and archaeological data in chronological and historical terms for this site.

## 2. Cañada Real archaeological site

The *Cañada Real* archaeological site is located in Caleruega (Burgos province, Spain: Fig. 1a). This site comprises a rectangular structure (7,2 x 5,8 m) enclosed by a short (0.5 m) stone wall, described as a medieval church by archaeological data (Fig. 1b). This site, located over a small hill, was studied during four different archaeological interventions in 2011, 2020, 2021 and 2022 (Palomino and Crespo 2021a, 2021b; Palomino and Crespo, 2022). During these campaigns, different occupational phases were distinguished, and some samples were collected in order to date them by radiocarbon.

The excavations carried out have identified a sequence of several phases of activity described below, from the earliest to the most recent, schematically illustrated in Fig. 1d. A human bone dated by $^{14}$C between 1497 to 1294 cal. BC at 2σ (stratigraphic unit UE126), along with the appearance of two prehistoric handmade ceramic fragments, indicate that the first human activities on the hill took place in the Late Bronze Age. These materials were found in a trench excavated in later stratigraphic units. In addition to this sporadic prehistoric presence, three main phases of medieval activity were identified. In phase I, a structure with an undefined floor plan and a mud and wood elevation was distinguished. It contained remains of a tamped clay surface, and its preservation was partially affected by later occupation phases. Post holes suggested a deck on wooden feet. It was not linked to prehistoric chronologies and had a $^{14}$C date of 564–650 cal AD (2σ), from a wood charcoal in stratigraphic unit UE137. The latter unit, UE137, is the

**Table 1**
Acceptance criteria for archaeointensity determinations:

| | Acceptance criteria for Thellier-Coe archaeointensity determinations | | | | | | | |
|---|---|---|---|---|---|---|---|---|
| Criteria | *N* | *f* | *q* | *β* | *δ (CK)* | *δ (pal)* | $MAD_{anc}$ (°) | *α* (°) |
| | ≥5 | ≥0.35 | ≥5 | ≤0.1 | ≤7 | ≤10 | ≤6 | ≤15 |

| | Acceptance criteria for Tsunakawa-Shaw archaeointensity determinations | | | | | |
|---|---|---|---|---|---|---|
| Criteria | $f_N$ | $r_N$ | $Slope_T$ | $f_T$ | $r_T$ | *k'* |
| | ≥0.15 | ≥0.995 | 0.95–1.05 | ≥0.15 | ≥0.995 | ≤0.2 |

**Note:** Thellier-Coe archaeointensity determinations, where *N*: number of successive measurement steps used for archaeointensity determination; *f*: fraction of NRM used; *q*: quality factor (Coe et al., 1978); β: ratio between standard error and absolute slope of the fit line; δ (CK): difference between the pTRM check and original TRM value at a given temperature, normalized to the TRM (Leonhardt et al., 2004); δ (pal): cumulative difference of the individual checks from room temperature up to the maximum temperature used for the best fit line (Leonhardt et al., 2003); $MAD_{anc}$ (°): mean angular deviation of anchored NRM; α (°): angular difference between vector average of the data selected for archaeointensity determination and the principal component of the data. Tsunakawa-Shaw archaeointensity determinations, where $f_N$: fraction used for the best fit line on the NRM-TRM1* plot; $r_N$: correlation coefficient for the best fit line on the NRM-TRM1* plot; $Slope_T$: slope of TRM1-TRM2* of the second heating; $f_T$: fraction used for the best fit line on the TRM1-TRM2* of the second heating; $r_T$: correlation coefficient for the best fit line on the TRM1-TRM2* of the second heating; *k*': curvature parameter of the NRM-TRM1*.

stratigraphic unit on which UE109, the burned structure dated here by archaeomagnetism, rests. Phase II featured a building with a rectangular floor plan and masonry walls. Its chronology is uncertain due to the absence of datable associated materials, but it is a building prior to the pre-Romanesque temple. The construction, use and abandonment of this small pre-Romanesque rural church would represent phase III (Fig. 1b and d). Although not dated by absolute methods, the similarities of the archaeological material (namely pottery) between phases II and III suggest a short time between them. In any case, this archaeomagnetic study dates UE109, which represents the abandonment of phase I, prior to the construction of the church.

## 3. Methodology

### 3.1. Archaeomagnetic sampling

To perform a full vector archaeomagnetic dating, twelve samples were collected from the stratigraphic unit UE109, as shown in Fig. 1c. Nine were magnetically oriented hand-block samples from the burned surface (numbers 2, 3, 5, 6, 7, 8, 9, 10 and 11), two were unoriented samples from the same burned surface (numbers 1 and 4) and one a single unoriented sample from the unburned area (number 12), considered as a baseline of the original sediment before the fire event.

The hand-blocks were sampled creating a horizontal surface with plaster and a piece of methacrylate, using two bubble levels and tracing magnetic north with a magnetic compass, once the plaster was hardened. These oriented samples were intended to be used for obtaining archaeomagnetic directions, but they have been also used for rock magnetic and absolute archaeointensity analyses. The unoriented samples were collected directly from the surface and kept in plastic bags, to be used just for archaeointensity and rock magnetic analyses.

### 3.2. Magnetic mineralogy analyses

To assess the suitability and reliability of these samples for archaeomagnetic analyses, several experiments were conducted to obtain information about the mineralogy and the magnetic carriers of the studied materials.

Three representative samples from the burned area were studied by Raman spectroscopy, to obtain a main mineralogy insight of the studied material and to relate it with the ferromagnetic mineralogy. The analyses were carried out in the CENIEH laboratory (Burgos, Spain) using an Olympus confocal optical microscope attached to a DXR Thermo Fisher Raman spectrometer. A near infrared laser, working at 780 nm wavelength was used with a laser power as low as 0.5 mW for avoiding mineral transformations owing to laser heating. Between 40–60 accumulations to 10 s exposure time were carried out to obtain the Raman spectra.

Five representative samples were chosen and powdered (~350 mg) to conduct coercivity and thermal analyses using the Variable Field Translation Balance (VFTB) at the Laboratory of Paleomagnetism of University of Burgos. The experiments included this sequence: progressive isothermal remanent magnetization (IRM) acquisition curves, hysteresis loops (± 1T), backfield coercivity curves and magnetization *vs.* temperature curves up to 700 °C. The results were interpreted with the *RockMagAnalyzer* software (Leonhardt, 2006).

Finally, two representative burned samples were studied with the Vibrating Sample Magnetometer (VSM) MicroMag 3900 to obtain domain state information of the magnetic carrier by measuring First Order Reversal Curves (FORCs), processed by *FORCinel* software (Harrison and Feinberg, 2008) applying a smoothing factor of 4. These analyses were conducted at the Marine Core Research Institute (MaCRI in Kochi, Japan).

### 3.3. Directional studies

The oriented hand-block samples were consolidated in the laboratory submerging them in a diamagnetic sodium silicate solution at 50 % for over an hour and left drying for one day. Subsequently, each hand-block was submerged in plaster, to obtain a plaster cube while preserving the original north magnetic mark traced in the field and left drying for several days. After that, the block was cut into cubic specimens of approximately 2 cm each side, preserving the original orientation. Specimens were named such as to specifically identify their location inside each hand block. It is important to highlight that the specimen's names with termination 01 come directly from the burned surface (from now on, surface specimens) while the termination 02 means that they belong to approximately 2 cm below (from now on, deeper specimens).

Six specimens from each hand-block sample (54 in total) were selected to perform the archaeomagnetic directional study. The natural remanent magnetization (NRM) of half of this set of specimens (27) was demagnetized using alternating field (AF) stepwise progressive demagnetization from 0 up to 90 or 105 mT. The other half set of samples (27 specimens) was stepwise thermally demagnetized from room temperature up to 600 °C. Both demagnetization methods were conducted at the Laboratory of Paleomagnetism of the University of Burgos, using a 2G SQUID magnetometer and a TD48-SC (ASC) thermal demagnetizer. The Characteristic Remanent Magnetization (ChRM) direction was calculated for the specimens by principal component analysis (Kirschvink, 1980) using the *Remasoft* software (Chadima and Hrouda, 2006). A mean archaeomagnetic direction for the site was obtained using Fisher (1953) statistics with the *PMagTools 4.2* software (Hounslow, 2006). The procedure consisted of first calculating a mean direction by hand-block and then, the common mean direction of all blocks, in a hierarchical

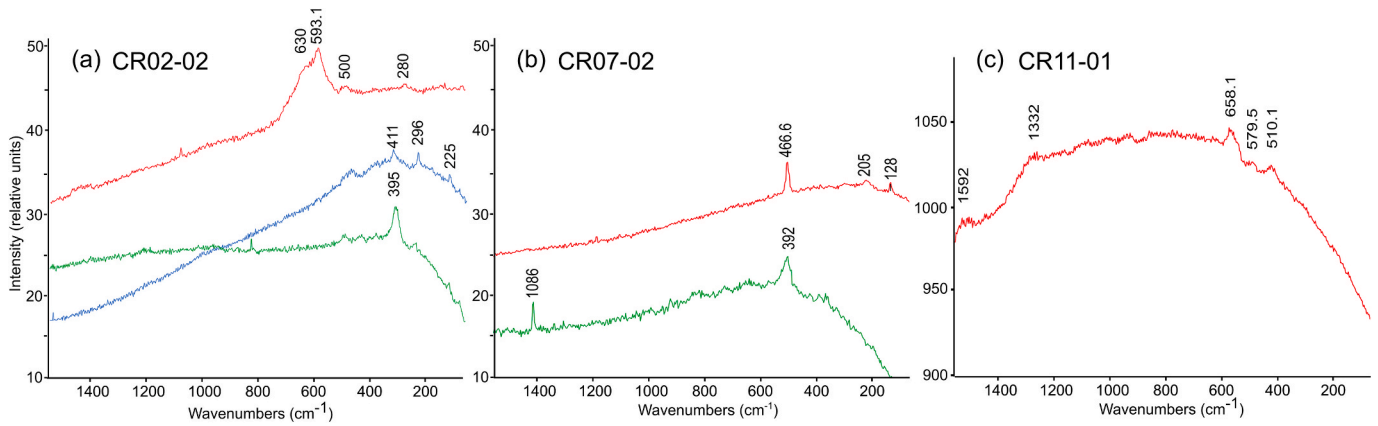


**Fig. 2.** Raman spectra obtained for samples (a) CR02-02, (b) CR07-02 and (c) CR11-01.

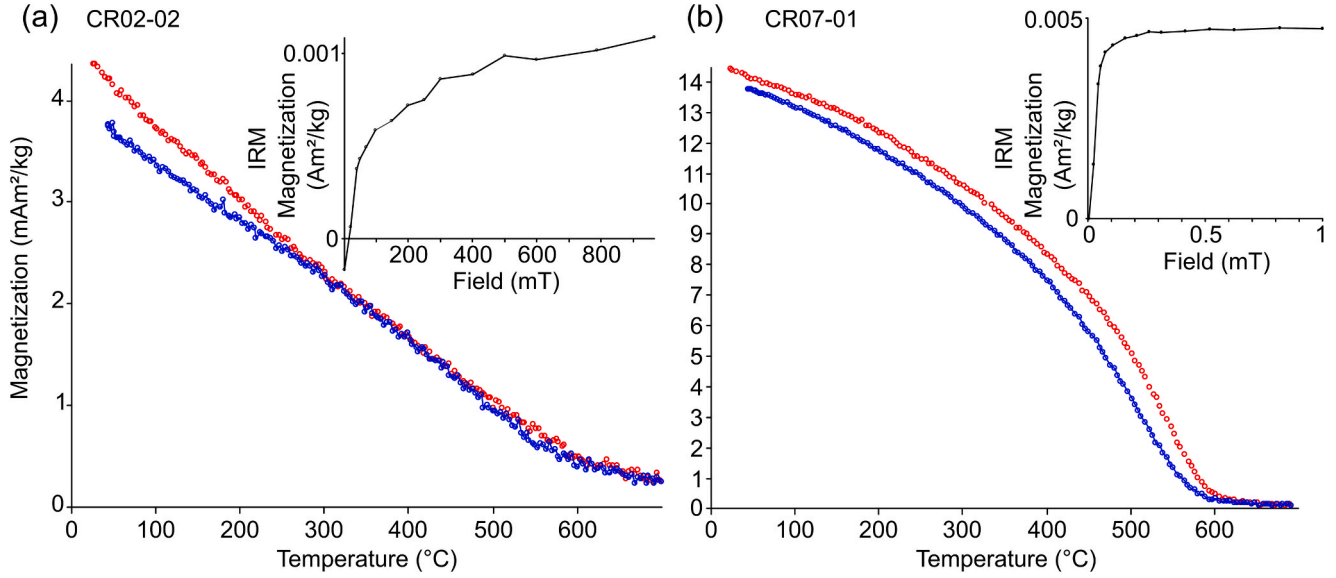


**Fig. 3.** Magnetization *vs*. temperature curves and its IRM acquisition curves for two representative samples of the two different thermomagnetic behaviours. (a) Sample CR02-02, from few centimetres below the burned surface. (b) Sample CR07-01, from the first centimetres of the burnt sediment. Heating cycle is shown in red and cooling cycle in blue.

approach (Lanos et al., 2005). Doing so decreases the effect of possible orientation errors in the field on the final result. Local declination correction was calculated for the entire collection using the 13th generation IGRF model (Alken et al., 2021) for the place and time of sampling. The declination correction was less than 1° and, therefore, it was considered negligible.

### 3.4. Archaeointensity methodologies

A multimethod approach was performed on this site to assess the applicability and suitability of different methods and, if possible, to compare their reproducibility. The methods applied were the Thellier-Coe method at the University of Burgos in Spain and the Tsunakawa-Shaw method at the MaCRI in Japan.

The Thellier-Coe method (Thellier and Thellier, 1959; Coe, 1967) was applied on 22 specimens from the burned surface samples, which demonstrated to be more suitable for archaeointensity studies. The specimens were prepared fixing chips by means of potassium silicate into diamagnetic cylindrical boron silicate vials of 10 mm diameter with an orientation mark. Several double temperature steps (zero-field and in-field), from room temperature up to 580 ℃ were measured, applying a 40 μT laboratory field for the in-field steps. In all the heating steps, samples were left 10 min at the goal temperature and then cooled down naturally for several hours. Multiple pTRM-checks were performed along the temperature sequence to detect possible thermal alterations. Measurements were performed using a 2G SQUID magnetometer and the heating steps were carried out using a TD48-SC (ASC) thermal demagnetizer, coupled with an argon insulated chamber. All heating processes were performed in an argon atmosphere, to prevent possible oxidation induced by the heating experiments. The results obtained were processed using the *ThellierTool 4.2* software (Leonhardt et al., 2004), using acceptance criteria included in this software (Paterson et al. 2014), shown in Table 1. Furthermore, to evaluate the existence of remanent magnetization carried by multidomain (MD) grains, the shape of the Arai plots was assessed, excluding from further interpretation those clearly showing a concave shape.

The Tsunakawa-Shaw method, which has also been previously applied to archaeological materials (e.g. Kitahara et al. 2018, Yamamoto et al. 2015, Vernet et al. 2025), was performed on 2 specimens (from samples CR02 and CR07), prepared in chip samples and placed in plastic cubes fixed using quartz fiber for the demagnetization steps. The procedure applied in the present study is detailed in Yamamoto and Tsunakawa (2005) and Yamamoto et al. (2015), where six progressive AF demagnetizations are performed from 0 up to 180 mT, at 2–10 mT

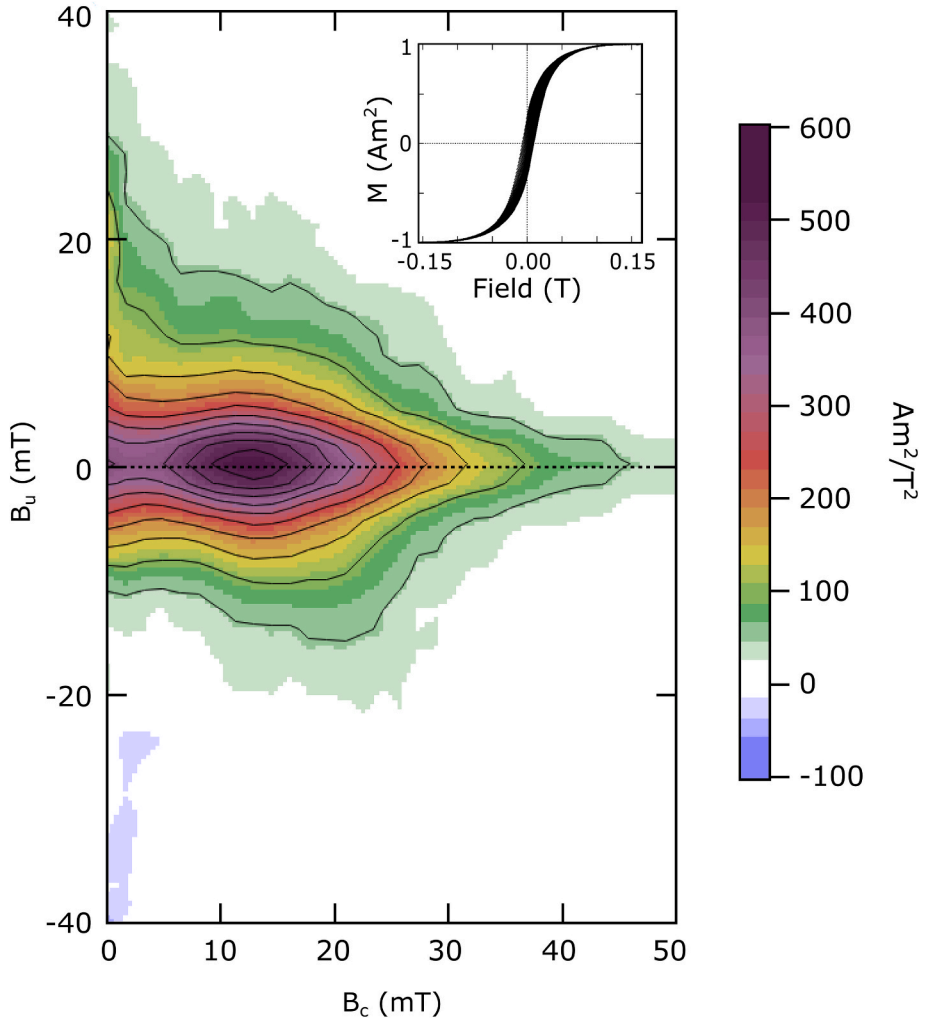


**Fig. 4.** First Order Reversal Curves (FORCs) diagram for sample CR07-01 and its corrected hysteresis loops. Smoothing factor used is 4.

intervals, using a DSPIN spinner magnetometer with an AF demagnetizer (Natsuhara Giken); two thermoremanent magnetizations (TRM) are imparted by heating the specimen in vacuum at a maximum temperature of 610 °C, during 10 min for the first TRM (TRM1) and 20 min for the second TRM (TRM2), applying a laboratory field of 40 μT, and cooling samples down to room temperature with a fan. In addition, low temperature demagnetizations (LTD) were conducted before each progressive demagnetization submerging the specimens in a dewar filled with liquid nitrogen (−192 °C) for 2 min, then taking them out of the dewar and let them heat up until room temperature was reached inside a magnetically shielded device. LTDs are applied to remove the contribution of MD-like remanences (Yamamoto et al., 2003). Anhysteretic remanent magnetizations (ARM) were imparted after each NRM or TRM demagnetization to apply an ARM correction for the final absolute paleointensity determination. ARM was imparted approximately parallel to the main NRM or TRM directions, using a bias field of 50 μT with an AF peak at 180 mT. The results were analyzed using the code developed by Yamamoto et al. (2022) run by the *PmagPy* software package (Tauxe et al., 2016). The applied acceptance criteria, recommended by Kitahara et al. (2018), are shown in Table 1.

## 4. Results and discussion

### 4.1. Magnetic mineralogy

#### 4.1.1. Raman spectroscopy

The results of the Raman spectroscopy performed on three burned samples are shown in Fig. 2: two are deeper specimens (Fig. 2a and b) and one surface specimen (Fig. 2c). Raman spectroscopy can identify magnetic and non-magnetic minerals. In sample CR02-02 (Fig. 2a), the bands on the red spectra have been interpreted as Mn oxides, the ones on the blue spectra as hematite and on the green spectra as goethite. In sample CR07-02 (Fig. 2b), the red spectra bands have been identified as quartz, and the green spectra as calcite with a band at 392 $cm^{-1}$ assigned to goethite. Lastly, the single red spectra in sample CR11-01 (Fig. 2c) shows bands interpreted as Mn oxides and others as carbon.

Some of the identified minerals, such as quartz, calcite and carbon, are diamagnetic, which means that they do not hold remanent magnetization in these samples. On the other hand, Mn oxide displays paramagnetic behaviour at room temperature (Ullah et al., 2018). This means that they will only show magnetization when a magnetic field is applied and decay to zero once the applied field is switched off. Therefore, they are not able to carry any magnetic remanence. Finally, hematite and goethite are known as antiferromagnetic minerals and have the capability to carry a magnetic remanence. In addition, these minerals typically display high coercivities and weak magnetization in comparison with ferrimagnetics (Dekkers 2007).

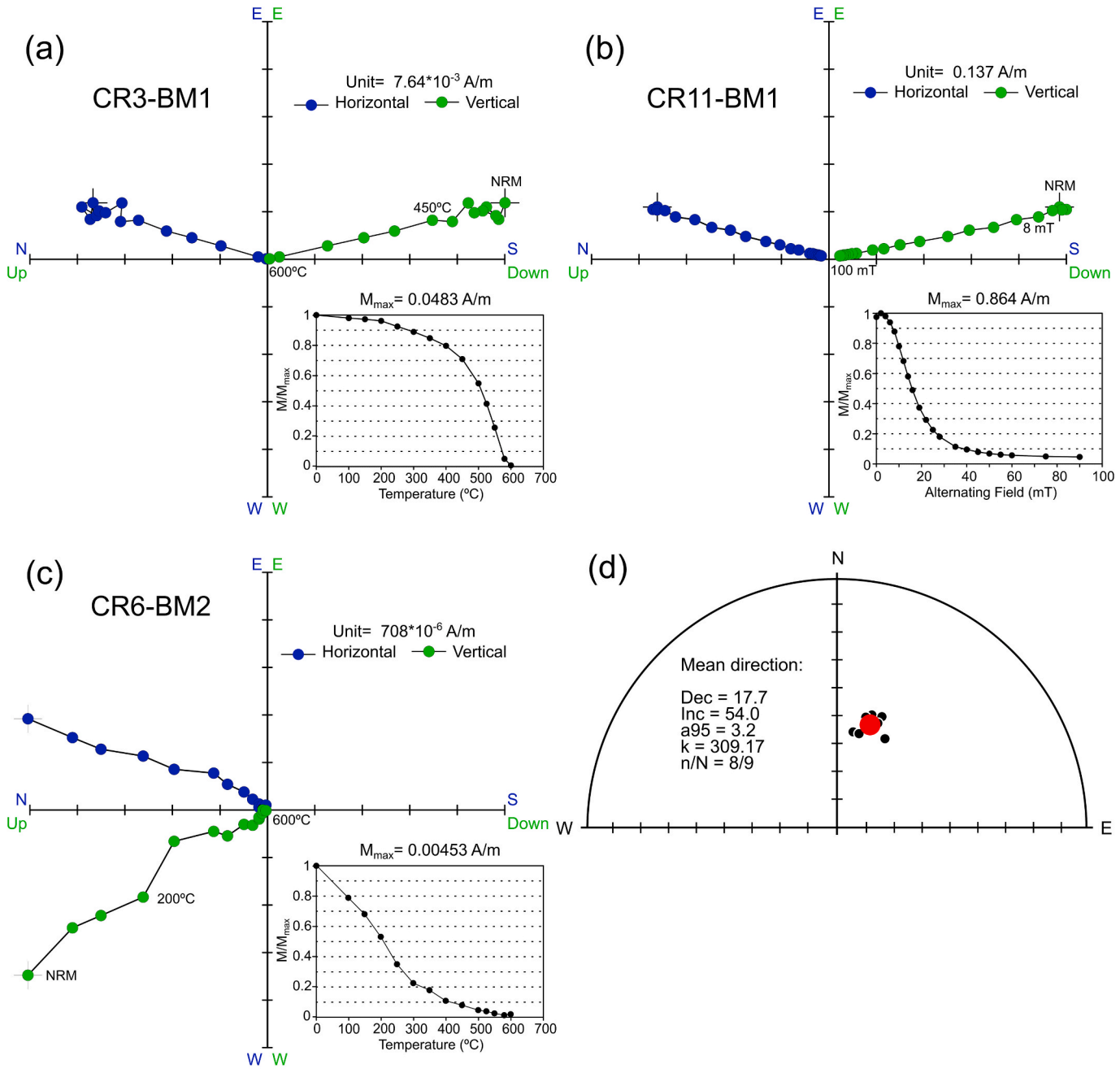


**Fig. 5.** (a-b) Representative orthogonal NRM demagnetization diagrams of two surface specimens, cleaned by AF (a) and thermal demagnetization (b), respectively. Blue (green) circles show projections of vector endpoints onto the horizontal (vertical) plane. The specimen code, intensity and normalized intensity decay curves are shown for both examples. (c) Representative orthogonal NRM demagnetization diagram of a deeper specimen, cleaned by thermal demagnetization. (d) Stereographic projection of the mean directions obtained per hand-block, with the mean direction of the site and its $\alpha_{95}$ (in red). Directional results and their corresponding statistical parameters are also shown. Dec. = declination; Inc. = inclination. α95 = 95 % confidence cone of mean direction; k = precision parameter according to Fisher (1953). n/N = number of samples accepted to calculate the mean direction / number of samples analyzed.

*4.1.2. Rock magnetic experiments*

The rock magnetic results obtained with the VFTB of two representative examples of deeper and surface specimens are displayed in Fig. 3. Fig. 3a is from a deeper specimen from the hand-block sample CR02. It displays low magnetization values and high coercivity, considering its unsaturated IRM curve even at 1 T. This high-coercivity phase is hematite according to the $T_C$ close to 675 °C identified in the thermomagnetic curve (Fig. 3a), which is also compatible with the Raman spectroscopy results (Fig. 2a and b). Goethite, which was identified with Raman spectroscopy, could not be observed in thermomagnetic experiments, suggesting that it might carry only a low proportion of the total magnetization. In addition, the occurrence of a phase with $T_C$ close to 580 °C (magnetite) cannot be ruled out, but it is not so evident. The features observed in Fig. 3a are very similar to those observed in other deeper specimens, as well as those from sample CR12, the unburned sample collected outside of the burned area. This fact indicates that specimens extracted from deeper levels of the direct burned surface are less affected or completely unaffected by heating and do not carry a TRM.

Fig. 3b belongs to a representative surface specimen. It displays high

**Table 2**
Mean directional results per hand-block sample and mean direction for the burned surface in Cañada Real archaeological site.

| Sample | Dec () | Inc () | $\alpha_{95}$ | k | n/N |
|---|---|---|---|---|---|
| CR02 | 9.5 | 57.7 | 4.3 | 805 | 3/6 |
| CR03 | 17.1 | 50.6 | 3.2 | 448.7 | 6/6 |
| CR05 | 14.5 | 51.9 | 4.1 | 514.4 | 4/6 |
| CR06 | 21.9 | 50 | 15 | 277.53 | 2/6 |
| CR07 | 21.2 | 52.6 | 4.5 | 219.5 | 6/6 |
| CR08 | 13.1 | 57.9 | 2.9 | 538.9 | 6/6 |
| CR09 | 28.1 | 56.4 | 5.8 | 132.8 | 6/6 |
| CR10 | – | – | – | – | 0/6 |
| CR11 | 15.1 | 53.7 | 2.8 | 578.9 | 6/6 |
| *Mean direction* | 17.7 | 54.0 | 3.2 | 309.2 | 8/9 |

**Note**: n/N: number of specimens considered for the directional calculation *vs.* number of specimens analyzed; Dec (°): declination; Inc (°): inclination; $\alpha_{95}$: confidence limit of the ChRM at 95% level (°); *k*: precision parameter (Fisher, 1953).

magnetization values (at least four times more intense than sample CR02-02, in Fig. 3a). The IRM acquisition curve saturates at low fields (around 150 – 200 mT), which is compatible with low coercivity minerals. The thermomagnetic curve is reversible with a clear inflection at ~600 °C, indicating magnetite or partially oxidized (maghemitized) magnetite as main magnetic carriers. Although the presence of magnetite could not be identified through Raman experiments for the surface specimen (Fig. 2c), it does not necessarily imply that it is not present as Carrancho et al. (2019) showed in an experimental study. Raman experiments study the main mineralogical phases in the sample, and magnetite can be the main magnetic carrier even if its proportion is very low. In fact, to reach the same magnetic intensity, about 200 times more hematite than magnetite is needed (Evans and Heller 2003). However, the observed magnetic properties clearly demonstrate the presence of magnetite as the main carrier of the magnetic remanence.

A FORC diagram with its corresponding set of hysteresis loops of sample CR07 is shown in Fig. 4. Such experiments can give information about the magnetic domain state of the sample, which has been chosen as representative of a burned surface specimen. The central coercivity peak with closed contours around ~12 mT and a central ridge indicates that single-domain (SD) low-coercivity particles are present (Roberts et al. 2000; Carvallo et al. 2006), while the features of the open external contours have been described as characteristic of single-vortex (SV) particles, known as pseudo single-domain (PSD) particles (Roberts et al. 2018). There is no significant interaction along the $B_u$ axis (elongated contours parallel to the y-axis), which excludes the dominant presence of multidomain particles. Since MD particles can disrupt the archaeointensity results obtained through Thellier-type experiments, this fact indicates that this kind of specimen seems to be suitable for archaeomagnetic experiments.

### 4.2. Archaomagnetic directions

All 54 oriented specimen results have been analyzed using their orthogonal NRM demagnetization plots to determine the characteristic remanent magnetization (ChRM) direction. Based on rock-magnetic data and further data provided below, this ChRM direction is considered to carry a TRM acquired during the cooling of the last heating event. Two different behaviors during the NRM demagnetization have been observed. Firstly, most specimens show a weak normal polarity viscous component removed at low fields (< 8 – 10 mT) or maximum unblocking temperatures of around < 350 °C. In 39 out of 54 specimens it was possible to isolate a normal polarity component defined between 10–100 mT by alternating field demagnetization and between 250 and 300 to 600 °C by thermal demagnetization. This component was considered to be the ChRM and shows a highly reproducible mean direction (Fig. 5a-b). Secondly, in a few cases (15 specimens), the specimens showed an erratic NRM demagnetization behavior, with very unstable magnetization and anomalous directions, therefore, they have not been considered to carry this ChRM (Fig. 5c). These specimens come

**Table 3**
Thellier-Coe and Tsunakawa-Shaw archaeointensity results for the Cañada Real archaeological site.

Thellier-Coe archaeointensy determinations

| Specimen | Class | $T_{min}$ – $T_{max}$ (°C) | N | f | δ (CK) | δ (pal) | q | $MAD_{anc}$ (°) | α (°) | B (μT) | $\Delta_b$ (μT) |
|---|---|---|---|---|---|---|---|---|---|---|---|
| CR02A | A | 350–580 | 10 | 0.81 | 5.9 | 4.8 | 14.99 | 4.6 | 3.5 | 33.1 | 1.5 |
| CR02B | A | 350–580 | 10 | 0.85 | 2.8 | 0.5 | 12.42 | 2.6 | 0.8 | 32.8 | 1.9 |
| CR02C | A | 350–580 | 10 | 0.87 | 3.6 | 3.4 | 15.4 | 2.2 | 0.6 | 45.9 | 2.2 |
| CR03A | A | 350–580 | 10 | 0.77 | 6.8 | 8.8 | 9.36 | 3.8 | 3.4 | 28.7 | 2.0 |
| CR03B | A | 350–580 | 9 | 0.87 | 4.1 | 2.2 | 13.26 | 2.7 | 1.2 | 32.3 | 1.7 |
| CR03C | A | 350–580 | 10 | 0.83 | 5.2 | 1.4 | 25.69 | 4.3 | 0.5 | 55.8 | 1.6 |
| CR05A | R | 350–580 | 9 | 0.69 | 4.8 | 5.7 | 9.04 | 2.7 | 0.3 | 7.6 | 0.5 |
| CR05B | R | – | – | – | – | – | – | – | – | – | – |
| CR05C | R | – | – | – | – | – | – | – | – | – | – |
| CR05D | R | 350–580 | 10 | 0.74 | 7 | 1.4 | 8.85 | 4.5 | 4.6 | 15.4 | 1.1 |
| CR06A | R | 350–580 | 9 | 0.82 | – | – | 5.57 | 7.6 | 6.0 | 17.5 | 2.1 |
| CR07A | R | 350–580 | 10 | 0.84 | 8.5 | 4.8 | 11.58 | 3.2 | 0.0 | 57.2 | 3.6 |
| CR07B | R | 350–580 | 10 | 0.88 | 10.4 | 1.5 | 9.8 | 2.3 | 0.3 | 48.3 | 3.7 |
| CR07C | R | 350–580 | 9 | 0.79 | 5.1 | 11.5 | 19.87 | 4.2 | 3.7 | 51.6 | 1.7 |
| CR07D | A | 350–580 | 9 | 0.91 | 2.5 | 2.5 | 11.67 | 5.6 | 3.7 | 35.0 | 2.4 |
| CR08A | A | 350–580 | 9 | 0.83 | 4.8 | 8.9 | 20.70 | 3.4 | 2.4 | 40.9 | 1.4 |
| CR08B | R | 350–580 | 9 | 0.83 | 10.6 | 20.2 | 12.74 | 5.8 | 2. | 54.8 | 3.0 |
| CR09A | R | – | – | – | – | – | – | – | – | – | – |
| CR09B | R | – | – | – | – | – | – | – | – | – | – |
| CR09C | R | 350–580 | 10 | 0.78 | 7.3 | 1.5 | 10.6 | 2.1 | 1.5 | 34.8 | 2.2 |
| CR11A | R | 350–580 | 9 | 0.84 | – | – | 5.34 | 3.8 | 3.8 | 14.8 | 2.0 |
| CR11B | R | 350–580 | 9 | 0.16 | – | – | 4.60 | 4.5 | 3.2 | 15.8 | 2.6 |

Tsunakawa-Shaw archaeointensity determinations

| Specimen | Class | $mT_{min}$-$mT_{max}$ | $f_N$ | $r_N$ | k' | $Slope_T$ | $f_T$ | $r_T$ | B (*μT*) | $\Delta_b$ (*μT*) |
|---|---|---|---|---|---|---|---|---|---|---|
| CR02D | R | 12–55 | – | 0.994 | 0.238 | 2.074 | – | 0.993 | – | – |
| CR07E | R | 6–180 | 0.912 | 0.996 | 0.206 | 1.643 | 0.937 | 0.999 | – | – |
| Mean A specimens | 8/22 | | | | | | | | 38.1 | 9.0 |

Note: A: specimens passing the acceptance criteria; R: discarded specimens. $T_{min}$ – $T_{max}$: temperature range selected in the Arai diagram for each archaeointensity determination; $mT_{min}$ – $mT_{max}$: alternating field range selected for each archaeointensity determination; B: estimated absolute archaeointensity; $\Delta_b$: uncertainty associated to each intensity determination. The remaining parameters are defined in Table 1.

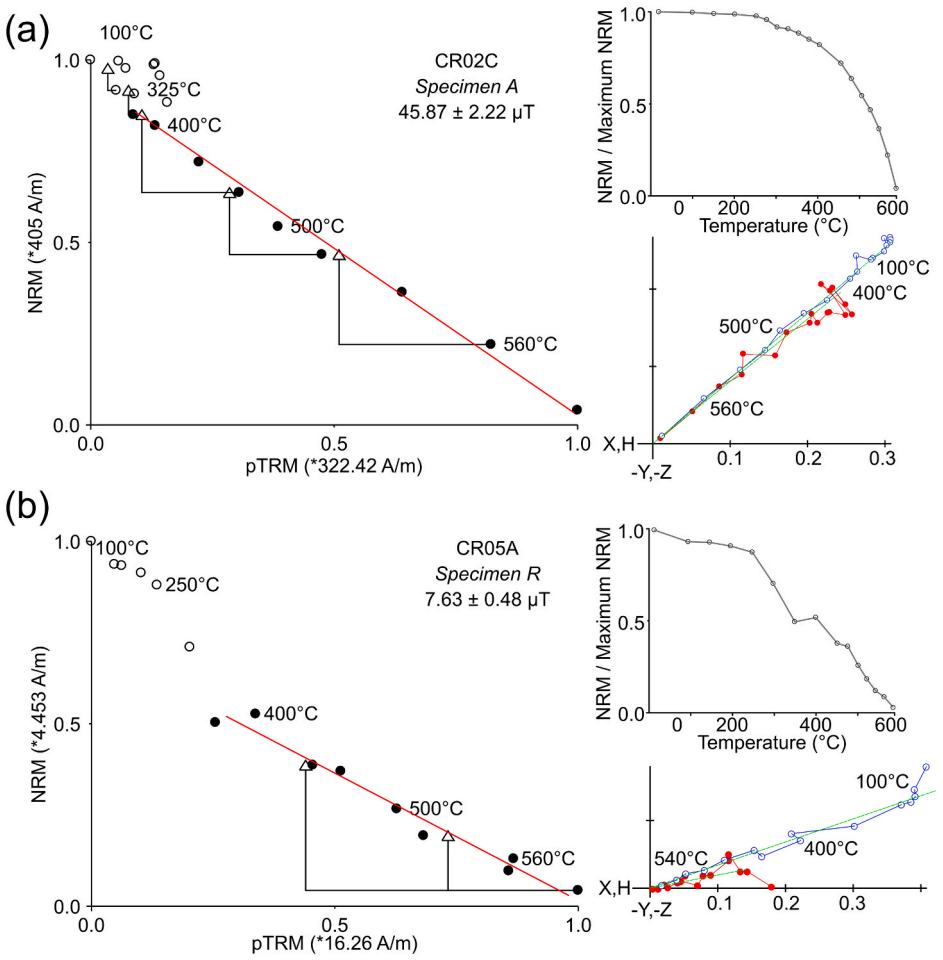


**Fig. 6.** Arai plots of the Thellier-Coe archaeointensity experiments obtained with the ThellierTool 4.2 software (Leonhardt et al., 2004). (a) Representative example of an accepted specimen with its best fit line. (b) Representative example of the discarded specimen CR05A.

from sample CR10 and deeper specimens (see appendix 1 and 2).

The Qn ratio (Koenigsberger 1938; Stacey 1967), a parameter commonly used in archaeomagnetism to assess whether a sample set carries a TRM, relates the remanent and induced magnetization as follows: Qn ratio = NRM / ($\chi$ ·H), with H being the local field strength (39 A/m). For these specimens, the resulting Qn ratios showed a wide range of values, with a clear cut that clusters the specimens in two groups. A first group with a Qn ratio below 2 (from 0.5 to 1.7) and a second group with higher Qn values ranging from 6.7 to 17.1 (see appendix 1 and 2). The latter group comprises all the surface specimens except those from sample CR10. This suggests that these specimens carry a TRM, in agreement with other archaeomagnetic studies performed on similar materials (e.g.: Hervé et al., 2011, García-Redondo et al. 2019). This demonstrates that, in this case, only the shallowest few centimeters in the sediment are able to acquire a TRM after a fire event, as has been observed in other previous studies (Calvo-Rathert et al., 2012). These results agree with the rock-magnetic experiments performed on surface specimens (strongly magnetic and dominated by magnetite; Fig. 3b) and deeper specimens (with weak magnetization values; Fig. 3a), as discussed in section 4.1.2. The Qn ratio has been previously used in archaeomagnetic studies to exclude specimens not carrying a TRM (e.g.: Carrancho et al. 2012, Kapper et al. 2014; Ertepinar et al. 2016). Considering our results, specimens from sample CR10 along with non-surface specimens (> 2 cm of depth), have been discarded to calculate the mean archaeomagnetic direction.

The final mean direction for this site has been calculated hierarchically from 8 out of 9 hand-block samples and is: Declination = 17.7°, Inclination = 54.0°, $\alpha_{95}$ = 3.2°, $k$ = 309.2 (Table 2 and Fig. 5d).

### 4.3. Archaeointensity results

The results obtained through the Thellier-Coe method are shown in Table 3 and representative examples illustrated in Fig. 6a-b. After applying the acceptance criteria displayed on Table 1 and discarding one sample with concave-shaped Arai plot (specimen CR05A, Fig. 6b), 8 out of 22 specimens were accepted, implying a success rate of 36 %. All specimens not passing the acceptance criteria yielded unacceptable values for the criteria related to pTRM checks: δ(CK) and δ(pal). These suggest possible thermal alteration produced during the heating experiments for the unsuccessful specimens. The temperature range applied to calculate the intensity value in the Arai plots for the whole set of specimens is between 350 to 580 °C. This range was shown to yield the best-fit line in the Arai plots and demonstrates homogeneous behavior for the successful specimens (Fig. 6a).

Tsunakawa-Shaw experiments, performed on two specimens, did not yield any successful intensity result (Table 3), as they were discarded by the acceptance criteria shown in Table 1. The plot in Fig. 7 shows the results of one of the specimens (Fig. 7a-b) and the normalized demagnetization for the different demagnetization procedures of this method (Fig. 7c) for the same specimen, along with its Median Destructive Field (MDF). The demagnetization of the NRM and TRM procedure steps show coercivity spectra analogous to the demagnetization once an ARM procedure is applied. After the first TRM (TRM1) is applied for 10 min, the MDF changes from 13 mT to over 30 mT, indicating large thermal alteration. Although smaller, this alteration also occurs after the second TRM (TRM2), as shown in Fig. 7b, which is performed for longer time (20 min) to identify further thermal alterations. As discussed above for

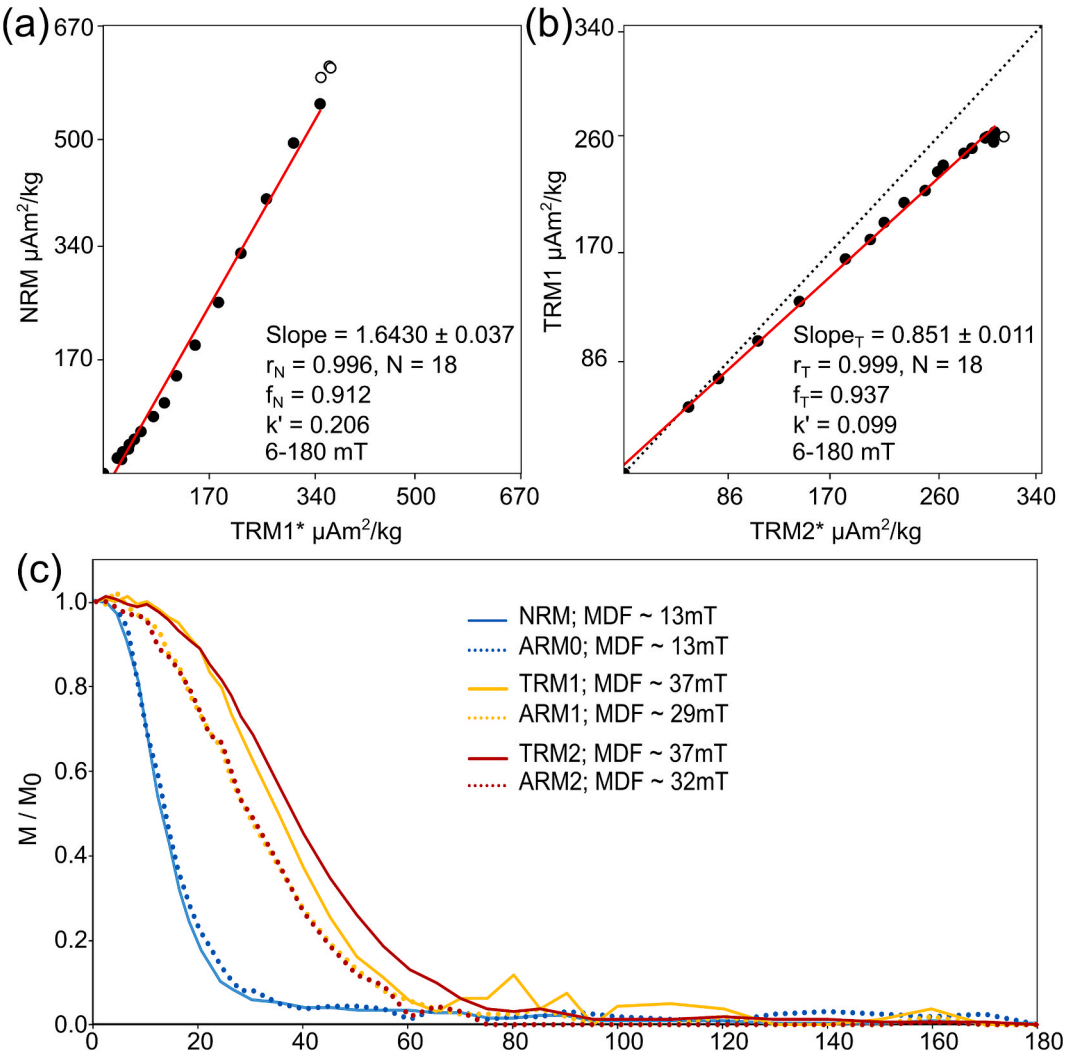


**Fig. 7.** Plots for the Tsunakawa-Shaw archaeointensity experiments. (a) Ratio between NRM and the first TRM* (*after ARM correction), yielding a potential archaeointensity estimate. (b) Plot of the first TRM* versus the second TRM* (*after ARM correction). (c) Normalized magnetization values along the Alternating Field demagnetization for NRM, ARM0, TRM1, ARM1, TRM2 and ARM2 (after subtraction of the 180 mT baseline) and its median destructive field (MDF), showing a divergence on the MDF and, therefore, the demagnetization shape, after the first TRM is applied.

some of the specimens subjected to the Thellier-Coe method, thermal alteration can affect differently in the studied specimens, this might be the reason why Tsunakawa-Shaw experiments were not successful in this case. Because of the unsuccessful results with Tsunakawa-Shaw experiments, the comparison of successful results obtained by two different methods could not be done.

Therefore, the final mean intensity value considered for the archaeomagnetic dating was the one obtained in Thellier-Coe experiments (Table 3), giving a result of 38.1 ± 9.0 μT. This value displays considerable dispersion. No strict consensus exists so far between different sets of acceptance criteria thresholds regarding within site scatter of paleointensity results, and the maximum allowed standard deviation to mean intensity ratio varies between 15 and 25 % (Cromwell et al., 2015; Sánchez-Moreno et al., 2020; Kissel and Laj, 2004; Selkin and Tauxe, 2000). Therefore, we consider that the relatively large 23.6 % within-site scatter of the present study can nevertheless still be considered acceptable.

### 4.4. Archaeomagnetic dating

To carry out the archaeomagnetic dating of the studied burned event in the Cañada Real site, the used archaeomagnetic direction was the hierarchical mean from hand-block samples, based only on the directions of the surface specimens showing a high Qn ratio value (see appendix 1 and 2). The archaeomagnetic directional results exhibit highly magnetic, univectorial and directionally reproducible orthogonal NRM diagrams (Fig. 5a-b), as well as high Qn ratio values (> 6). For the mean intensity value, Thellier-Coe determinations have been considered.

Full-vector archaeomagnetic dating was performed using the ArchaeoPyDating software (Serrano et al. 2024) with the SCHA.DIF.4k model (Pavón-Carrasco et al. 2021) at the site coordinates. This regional model covers geomagnetic data for the last 4 millennia, is well updated with full vector data and avoids the relocation error (Casas and Incoronato, 2007). A single age interval was obtained between 995 and 1125 CE at 95 % confidence (Fig. 8). It is therefore a medieval burning event. The relatively large scatter of the archaeointensity results implies that the archaeomagnetic dating is supported by the archaeomagnetic directional data. Although the archaeointensity data do not contribute to narrowing the limits of dating, they are in agreement with the results obtained from the directional data. Previous to this archaeomagnetic study performed on the stratigraphic unit UE109, two samples from older stratigraphic units were subjected to radiocarbon dating. One of the samples, a human bone from the stratigraphic unit UE126, yielded a

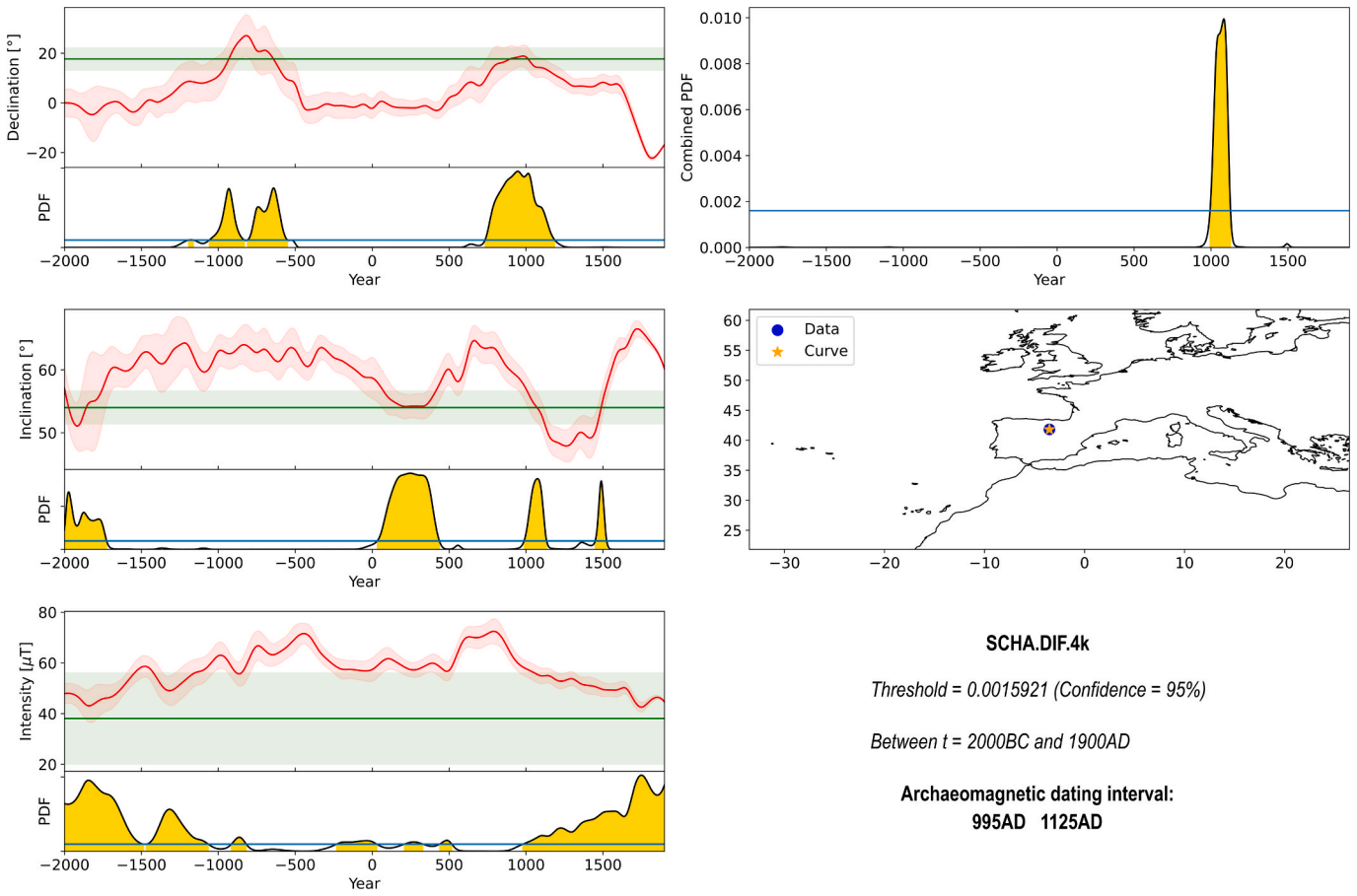


**Fig. 8.** Full vector archaeomagnetic dating results obtained for the studied burned level at Cañada Real site using the SCHA.DIF.4k geomagnetic model at 95 %. Dating was performed using ArchaeoPyDating (Serrano et al., 2024) The comparaison of each undated geomagnetic element (in green) and the reference curve (in red) is shown. Bands represent the uncertainties at 2σ. The probability density function (PDF) of each component is also shown, as well as the final dating provided by the combined PDF. Gold colored intervals define the 95 % of the total area enclosed by the PDFs. In the location map, the blue dot represents the location of the site and the orange star the origin coordinates of the reference curve.

dating result between 1497 to 1294 BCE, therefore corresponding to the Late Bronze Age (Fig. 1d). It seems clear that there was human activity in the Late Bronze Age because in addition to the human remains dated by $^{14}$C, there were also two prehistoric handmade ceramic fragments discovered in 2022. One of them comes from the stratigraphic unit UE150 (undated – phase III) and the other from the stratigraphic unit UE137. UE137 is the stratigraphic unit underlying the unit UE109, the burned surface studied here by archaeomagnetism. Both the human remains, and these pottery fragments are displaced from their original location and inserted in later sedimentary deposits. Most probably, the construction of the building with masonry walls and subsequently the church (phases II and III, respectively), generated some moving of previous materials.

The second radiocarbon dating, performed on a wood charcoal from stratigraphic unit UE137, yielded an age range between 564 to 650 yr AD (mid-6th to 7th century CE; Fig. 1d). The archaeomagnetic dating obtained from the burned stratigraphic unit (UE109) is also medieval: 995 – 1125 yr AD, but later. If both dates (radiocarbon and archaeomagnetic) are correct, between 4 and 6 centuries would have elapsed between the level on which the remains of the wooden post structures are laid (UE137 – start of phase I) and its closure and abandonment with a fire (UE109 – end of phase I). There is no archaeological evidence available to explain this wide time interval, but these results deserve a comment. Unlike radiocarbon, it should be noted that archaeomagnetism dates the last heating (e.g.: Tauxe et al. 2010). In this particular case, what is being dated is the potential abandonment of Phase I (Fig. 1d). In addition, the radiocarbon sample from UE137 could have been affected by the "old wood effect" (Schiffer 1986). This happens when the dated charcoal corresponds to wood from an older building or the innermost part of a large trunk. If so, that would imply that the $^{14}$C dating would be aged by some decades or even centuries. That is why it is better to use, when available, short-lived samples such as seeds, shells or bones for radiocarbon dating. At present, this possibility cannot be ruled out. In any case, the radiocarbon date of UE137 should be considered as a *terminus post-quem* for the construction of the mud and wooden structure (start of Phase I).

Phase II corresponds to a later time where a rectangular building with masonry walls is identified. It is not chronometrically dated but is stratigraphically earlier than the pre-Romanesque church of phase III (Fig. 1d). The typological and decorative similarities observed between the medieval ceramics found in Cañada Real and those recovered at the neighbouring site of La Pudia I (García-Redondo et al. 2020), indicate that the construction of the church (phase III) was around the mid-11th – early 12th century CE (Palomino and Crespo, 2021b). Considering the dates of the archaeomagnetic dating obtained here for the end of Phase I (end 10th – first third of the 12th century CE) and the construction of the church (mid-11th – early 12th century CE), the Phase II building must have been short-lived, destroyed when the church was built in Phase III.

Likewise, it is not possible to prove it, but it is tempting to associate these dates and the destruction of the structure of phase I (here dated) with one of the Muslim *aceifas* or *razzias* (e.g.: 1003 CE), which are historically documented (Bramon, 1995). Although archaeomagnetic dating is not yet as widespread as other geochronological techniques

such as $^{14}C$, it is undoubtedly of great value for the interpretation of archaeological contexts with burned materials.

## 5. Conclusions

An archaeomagnetic study has been performed in the burned surface UE109 in Cañada Real archaeological site, including rock-magnetic, archaeomagnetic and archaointensity experiments on this burned surface, to date the fire event. The following conclusions can be drawn from this study:

- The Qn ratio and rock magnetic experiments displayed different features on burned (surface specimens) and non-burned sediments (deeper than 2 cm specimens or specimens coming from peripherical samples). This allowed to distinguish and select specimens carrying a TRM (the most superficial and best burned), which are suitable for this archaeomagnetic study.
- Archaeomagnetic studies were performed on 54 specimens from 9 handblocks with both alternating field and thermal demagnetization. Only specimens with high Qn ratio values ($> 6$) displaying highly magnetic, univectorial demagnetization diagrams were selected for calculating a final mean direction. The final mean direction, calculated hierarchically, yields the following result: declination $= 17.7^{\circ}$, inclination $= 54.0^{\circ}$, $\alpha_{95} = 3.2^{\circ}$, $k = 309.2$, n $= 8$ hand-blocks (out of 9 measured).
- Archaeointensity determinations were performed with both the Thellier-Coe and the Tsunakawa-Shaw methods. A mean intensity value of 38.1 $\pm$ 9.0 μT was obtained only from the successful Thellier-Coe specimens.
- Full vector archaeomagnetic dating was performed using the geomagnetic field model SCHA.DIF.4 k. A single time interval between 995 and 1125 CE (95 % of confidence) was obtained as the date of the fire event that produced the studied burned surface. This event is related with the abandonment of one of the phases of occupation (phase I) and is in good agreement with previous stratigraphic constrains.
- It cannot be ruled out that this fire was produced by one of the Muslim *razzias* documented at the end of the 10th – beginning of the 11th century CE. This study is a good testimony of how the combination of various geochronological techniques and archaeological data contribute to reconstruct the occupation history of a site, and particularly archaeomagnetism, to date the last burning of combustion events.

## CRediT authorship contribution statement

**Eva Vernet:** Conceptualization, Formal analysis, Investigation, Writing - Original Draft, Writing - Review & Editing, Visualization. **Ángel Carrancho:** Conceptualization, Formal analysis, Writing - Review & Editing, Supervision, Project administration, Funding acquisition. **Manuel Calvo-Rathert:** Conceptualization, Formal analysis, Writing - Review & Editing, Supervision, Project administration, Funding acquisition. **Yuhji Yamamoto:** Software, Formal analysis, Writing - Review & Editing, Supervision. **Susana E. Jorge:** Formal analysis, Writing - Review & Editing. **María F. Bógalo:** Formal analysis, Writing - Review & Editing. **Ángel Palomino:** Resources, Writing - Review & Editing.

## Declaration of competing interest

The authors declare that they have no known competing financial interests or personal relationships that could have appeared to influence the work reported in this paper.

## Acknowledgements

We would like to acknowledge *Cañada Real* excavation staff for their help in the sampling campaign, as well as Caleruega municipal council. This research has been supported by project PID2019105796GB-I00 of the Agencia Estatal de Investigación and project BU037P23 of the Junta de Castilla y León and the European Regional Development Fund. Eva Vernet Tarragó acknowledges funding from PRE2020-094803 (Agencia Estatal de Investigación) contract. We sincerely appreciate the comments of the Editor and two anonymous reviewers, which have improved the manuscript. Dataset available on: doi: 10.5281/zenodo.15458528. This research paper is a component of Eva Vernet's PhD thesis, and all authors agree.

## Appendix A. Supplementary material

Supplementary data to this article can be found online at https://doi.org/10.1016/j.jasrep.2025.105278.

## Data availability

Dataset available on https://doi.org/10.5281/zenodo.15458528.

## References

Aidona, E., Kondopoulou, D., 2012. First archaeomagnetic results and dating of Neolithic structures in northern Greece. Stud. Geophys. Geod. 56, 827–844. https://doi.org/10.1007/s11200-011-9006-8.

Alken, P., Thébault, E., Beggan, C.D., Amit, H., Aubert, J., Baerenzung, J., Bondar, T., Brown, W.J., Califf, S., Chambodut, A., Chulliat, A., Cox, G.A., Finlay, C.C., Fournier, A., Gillet, N., Huder, L., Kloss, C., Livermore, P.W., Lowes, F.J., Macmillan, S., Magnes, W., Mandea, M., Marsal, S., Nair, M., Olsen, N., Pavón-Carrasco, F.J., Petrov, V.G., Rother, M., Sabaka, T.J., Sánchez, S., Saturnino, D., Schnepf, N.R., Stolle, C., Terra-Nova, F., Thomson, A.W.P., Toepfer, M., Tøffner-Clausen, L., Vigneron, P., 2021. International geomagnetic reference field: the thirteenth generation. Earth Planets Space 73, 49. https://doi.org/10.1186/s40623-020-01288-x.

Batt, C., 2023. Archaeomagnetic dating. In: Polard, A.M., Armitage, R.A., Makarewicz, C. A. Handbook of archaeological sciences, chapter 6, Wiley, pp. 99–117, doi: 10.1002/9781119592112.ch6.

Bramon, D., 1995. La batalla de Albesa (25 de febrero de 1003) y la primera aceifa de Ábd al-Mallk al-Muzaifar (verano del mismo año). Anaquel de Estudios Árabes VI, 21-27.

Calvo-Rathert, M., Carrancho, Á., Stark, F., Villalaín, J.J., Hill, M., 2012. Are burnt sediments reliable recorders of geomagnetic field strength? Quat. Res. 77 (2), 326–330. https://doi.org/10.1016/j.yqres.2011.11.001.

Carrancho, Á., Jorge-Villar, S.E., Sánchez-Romero, L., Karampaglidis, T., 2019. Combined study of archaeomagnetism and Raman spectroscopy of experimentally burnt limestones from the middle-palaeolithic site of Pinilla del Valle (Madrid, Spain). Bol. Soc. Geol. Mex. 71 (2), 383–396. https://doi.org/10.18268/BSGM2018v70n2a9.

Carrancho, Á., Gómez-Paccard, M., Pavón-Carrasco, F.J., 2022. Archaeomagnetic dating: fundamentals, achievements and limitations. Cuat. Geomorfol. 36 (3–4), 31–43.

Carrancho, Á., Villalaín, J.J., Vergès, J.M., Vallverdú, J., 2012. Assessing post-depositional processes in archaeological cave fires through the analysis of archaeomagnetic vectors. Quat. Int. 275, 14–22.

Carvallo, C., Roberts, A.P., Leonhardt, R., Laj, C., Kissel, C., Camps, P., 2006. Increasing the efficiency of palaeointensity analyses by selection of samples using first-order reversal curve diagrams. J. Geophys. Res. 111, B12103. https://doi.org/10.1029/2005JB004126.

Casas, L., Incoronato, A., 2007. Distribution analysis of errors due to relocation of geomagnetic data using the 'Conversion via Pole' (CVP) method: implications on archaeomagnetic data. Geophys. J. Int. 169, 448–454. https://doi.org/10.1111/j.1365-246X.2007.03346.x.

Chadima, M., Hrouda, F., 2006. Remasoft 3.0 a user-friendly palaeomagnetic databrowser and analyzer. Travaux Géophysiques XXVII, 20–21.

Coe, R.S., 1967. Paleointensities of the earth's magnetic field determined from tertiary and quaternary rocks. J. Geophys. Res. 72 (12), 3247–3262. https://doi.org/10.1029/JZ072i012p03247.

Coe, R.S., Grommé, S., Mankinen, E.A., 1978. Geomagnetic paleointensities from radiocarbon-dated lava flows on Hawaii and the question of the Pacific nondipol low. J. Geophys. Res. 83, 1740–1756.

Cromwell, G., Tauxe, L., Staudigel, H., Ron, H., 2015. Paleointensity estimates from historic and modern hawaiian lava flows using glassy basalt as a primary source material. Phys. Earth Planet. Inter. 241, 44–56. https://doi.org/10.1016/j.pepi.2014.12.007.

Dekkers M.J., 2007. Magnetic proxy parameters. In: D. Gubbins, E. Herrero-Bervera (eds.), Encyclopedia of Geomagnetism and Palaeomagnetism. Springer, 525-534.

Di Chiara, A., Pavón-Carrasco, F.J., 2022. A first regional model of the past Earth's magnetic field from Africa for the last 4000 years. Phys. Earth Planet. Inter. 325, 106855. https://doi.org/10.1016/j.pepi.2022.106855.
Dunlop, D.J., Özdemir, Ö., 1997. Rock Magnetism: Fundamentals and Frontiers. Cambridge Univ. Press, New York, 573 pp.
Ertepinar, P., Langereis, C.G., Biggin, A.J., de Groot, L.V., Kulakoglu, F., Omura, S., Suel, A., 2016. Full vector archaeomagnetic records from Anatolia between 2400 and 1350 BCE: implications for geomagnetic field models and the dating of fires in antiquity. Earth Planet. Sci. Lett. 434, 171–186. https://doi.org/10.1016/j.epsl.2015.11.015.
Evans, M.E., Heller, F., 2003. Environmental magnetism: principles and applications of environmagnetics, Academic Press, San Diego, CA. 299 pp.
Fisher, R., 1953. Dispersion on a sphere. Proc. R. Soc. Lond. Ser. A 217 (1130), 295–305. https://doi.org/10.1098/rspa.1953.0064.
García-Redondo, N., Carrancho, Á., Goguitchaichvili, A., Morales, J., Calvo-Rathert, M., Palomino, A., 2020. New constraints on the medieval repopulation process in the northern Iberian plateau from the full vector archaeomagnetic dating of two hearths at La Pudia site (Caleruega, Burgos, Spain). Archaeol. Anthropol. Sci. 12 (4), 91.
García-Redondo, N., Carrancho, Á., Goguitchaichvili, A., Morales, J., Palomino, A., 2019. Comprehensive magnetic surveys of kilns for bell and tile fabrication in Castile (Spain). J. Archaeol. Sci. Rep. 23, 426–436. https://doi.org/10.1016/j.jasrep.2018.11.003.
García-Ruiz, R., Goguitchaichvili, A., Pavon-Carrasco, F.J., Soler, A.M., Pérez-Rodríguez, N., Osete, M.L., Morales, J., Kravchinsky, V., 2022. Fluctuations of magnetic inclination and declination in Mexico during the last three millennia. Quat. Geochronol. 71, 101309. https://doi.org/10.1016/j.quageo.2022.101309.
Gomez-Paccard, M., Chauvin, A., Lanos, P., Mcintosh, G., Osete, M.L., Catanzariti, G., Ruiz-Martínez, V.C., Núñer, J.I., 2006. First archaeomagnetic secular variation curve for the Iberian Peninsula: Comparison with other data from Western Europe and with global geomagnetic field models. Geochem. Geophys. Geosyst. 7 (12).
Harrison, R.J., Feinberg, J.M., 2008. FORCinel: an improved algorithm for calculating first-order reversal curve distributions using locally weighted regression smoothing. Geochem. Geophys. Geosyst. 9, Q05016. https://doi.org/10.1029/2008GC001987.
Herrejón-Lagunilla, Á., Villalaín, J.J., Pavón-Carrasco, F.J., Sánchez-Bravo, M.S., Sossa-Ríos, S., Mayor, A., Galván, B., Hernández, C.M., Mallol, C., Carrancho, Á., 2024. The time between Palaeolithic hearths. Nature 630, 666–670. https://doi.org/10.1038/s41586-024-07467-0.
Hervé, G., Lanos, P., 2018. Improvements in Archaeomagnetic Dating in Western Europe from the late Bronze to the late Iron Ages: an Alternative to the Problem of the Hallstattian Radiocarbon Plateau. Archaeometry 60, 870–883. https://doi.org/10.1111/arcm.12344.
Hervé, G., Schnepp, E., Chauvin, A., Lanos, P., Nowaczyk, N., 2011. Archaeomagnetic results on three Early Iron Age salt-kilns from Moyenvic (France). Geophys. J. Int. 185 (1), 144–156.
Hounslow, M.W., 2006. PMag Tools v4.2a (http://geography.lancaster.ac.uk/cemp/cemp.htm).
Jordanova, N., Kovacheva, M., Kostadinova, M., 2004. Archaeomagnetic investigation and dating of Neolithic archaeological site (Kovachevo) from Bulgaria. Phys. Earth Planet. Int. 147, 89–102.
Kapper, K.L., Donadini, F., Mauvilly, M., Panovska, S., Hirt, A.M., 2014. New directional archeomagnetic data of burned cave sediments from Switzerland and geomagnetic field variations in Central Europe. Geophys. J. Int. 198 (2), 1208–1221. https://doi.org/10.1093/gji/ggu184.
Kirschvink, J.L., 1980. The least-squares line and plane and the analysis of palaeomagnetic data. Geophys. J. R. Astron. Soc. 62, 699–718. https://doi.org/10.1111/j.1365-246X.1980.tb02601.xj.
Kissel, C., Laj, C., 2004. Improvements in procedure and paleointensity selection criteria (PICRIT-03) for Thellier and Thellier determinations: application to Hawaiian basaltic long cores. Phys. Earth Planet. Inter. 147 (2–3), 155–169. https://doi.org/10.1016/j.pepi.2004.06.010.
Kitahara, Y., Yamamoto, Y., Ohno, M., Kuwahara, Y., Kameda, S., Hatakeyama, T., 2018. Archeointensity estimates of a tenth century kiln: first application of the Tsunakawa–Shaw paleointensity method to archaeological relics. Earth Planets Space 70, 79. https://doi.org/10.1186/s40623-018-0841-5.
Koenigsberger, J.G., 1938. Natural residual magnetism of eruptive rocks, Part II. Terr. Magn. Atmos. Electr. 43, 299–320.
Kovacheva, M., Kostadinova-Avramova, M., Jordanova, N., Lanos, P., Boyadzhiev, Y., 2014. Extended and revised archaeomagnetic database and secular variation curves from Bulgaria for the last eight millennia. Phys. Earth Planet. Inter. 236, 79–94. https://doi.org/10.1016/j.pepi.2014.07.002.
Lanos, P., Le Goff, M., Kovacheva, M., Schnepp, E., 2005. Hierarchical modelling of archaeomagnetic data and curve estimation by moving average technique. Geophys. J. Int. 160 (2), 440–476. https://doi.org/10.1111/j.1365-246X.2005.02490.x.
Leonhardt, R., Heunemann, C., Krasa, D., 2004. Analyzing absolute paleointensity determinations: Acceptance criteria and the software ThellierTool 4.0. Geochem. Geophys. Geosyst. 5 (12). https://doi.org/10.1029/2004GC000807.
Leonhardt, R., Matzka, J., Menor, E.A., 2003. Absolute paleointensities and paleodirections from Fernando de Noronha, Brazil. Phys. Earth Planet. Inter. 139, 285–303.
Leonhardt, R., 2006. Analyzing rock magnetic measurements: the RockMagAnalyzer 1.0 software. Comput. Geosci. 32, 1420–1431. https://doi.org/10.1016/j.cageo.2006.01.006.
Molina-Cardín, A., Campuzano, S. A., Osete, M. L., Rivero-Montero, M., Pavón-Carrasco, F. J., Palencia-Ortas, A., Martín-Hernández, F., Gómez-Paccard, M., Chauvin, A., Guerrero-Suárez, S., Pérez-Fuentes, J.C., MacIntosh, G., Catanzariti, G., Sastre Blanco, J.C., Larrazabal, J., Fernández-Martínez, V.M., Álvarez Sanchís, J.R., Rodríguez-Hernández, J., Martín-Viso, I., García i Rubert D., 2018. Updated Iberian archeomagnetic catalogue: New full vector paleosecular variation curve for the last three millennia. Geochem. Geophys. Geosyst. 19, 3637–3656, doi: 10.1029/2018GC007781.
Palomino Lázaro, Á.L., Crespo Díez, M., 2021a. Inedit archaeological report (in spanish): Trabajos de excavación arqueológica en el yacimiento de Cañada Real (Caleruega, Burgos). Noviembre-Diciembre de 2020. Informe técnico inédito depositado en el Servicio Territorial de Cultura de la Junta de Castilla y León en Burgos.
Palomino Lázaro, Á.L., Crespo Díez, M., 2021b. Inedit archaeological report (in spanish): Trabajos de excavación arqueológica en el yacimiento de Cañada Real (Caleruega, Burgos). Campaña 2021. Informe técnico inédito depositado en el Servicio Territorial de Cultura de la Junta de Castilla y León en Burgos.
Palomino Lázaro, Á.L., Crespo Díez, M., 2022. Inedit archaeological report (in spanish): "Trabajos de excavación arqueológica en el yacimiento de Cañada Real (Caleruega, Burgos). Campaña 2021. Informe técnico inédito depositado en el Servicio Territorial de Cultura de la Junta de Castilla y León en Burgos.".
Paterson, G.A., Tauxe, L., Biggin, A.J., Shaar, R., Jonestrask, L.C., 2014. On improving the selection of Thellier-type paleointensity data. Geochem. Geophys. Geosyst. 15, 1180–1192.
Pavón-Carrasco, F.J., Campuzano, S.A., Rivero-Montero, M., Molina-Cardín, A., Gómez-Paccard, M., Osete, M.L., 2021. SCHA.DIF.4k: 4,000 years of paleomagnetic reconstruction for Europe and its application for dating. J. Geophys. Res. Solid Earth 126, e2020JB021237. https://doi.org/10.1029/2020JB02123.
Roberts, A.P., Pike, C.R., Verosub, K.L., 2000. First-order reversal curve diagrams: anew tool for characterising the magnetic properties of natural samples. J. Geo-Phys. Res. 105, 28461–28475.
Roberts, A.P., Zhao, X., Harrison, R.J., Heslop, D., Muxworthy, A.R., Rowan, C.J., Larrasoaña, J.-C., Florindo, F., 2018. Signatures of reductive magnetic mineral diagenesis from unmixing of first-order reversal curves. J. Geophys. Res. Solid Earth 123, 4500–4522. https://doi.org/10.1002/2018JB015706.
Sánchez-Moreno, E.M., Calvo-Rathert, M., Goguitchaichvili, A., Tauxe, L., Vashakidze, G. T., Lebedev, V.A., 2020. Weak palaeointensity results over a Pliocene volcanic sequence from Lesser Caucasus (Georgia): transitional record or time averaged field? Geophys. J. Int. 220 (3), 1604–1618. https://doi.org/10.1093/gji/ggz533.
Schanner, M., Korte, M., Holschneider, M., 2022. ArchKalmag14k: a Kalman-filter based global geomagnetic model for the Holocene. J. Geophys. Res. Solid Earth 127 (2), e2021JB023166. https://doi.org/10.1029/2021JB023166.
Schiffer, M.B., 1986. Radiocarbon dating and the "old wood" problem: the case of the Hohokam chronology. J. Archaeol. Sci. 13, 13–30.
Selkin, P.A., Tauxe, L., 2000. Long-term variations in palaeointensity. Philos. Trans. R. Soc. A 358, 1065–1088. https://doi.org/10.1098/rsta.2000.0574.
Serrano, M., Pavón-Carrasco, F.J., Campuzano, S.A., Osete, M.L., 2024. ArchaeoPyDating: a new user-friendly release for archaeomagnetic dating. Archaeometry 66 (6), 1424–1437. https://doi.org/10.1111/arcm.13009.
Stacey, F.D., 1967. The koenigsberger ratio and the nature of thermoremanence in igneous rocks. Earth Planet. Sci. Lett. 2 (1), 67–68. https://doi.org/10.1016/0012-821X (67)90174-4.
Tauxe, L., 2010. Essentials of Rock and Paleomagnetism. University of California Press (1st Edit.), 512 pp.
Tauxe, L., Shaar, R., Jonestrask, L., Swanson-Hysell, N.L., Minnett, R., Koppers, A.A.P., Constable, C.G., Jarboe, N., Gaastra, K., Fairchild, L., 2016. PmagPy: software package for paleomagnetic data analysis and a bridge to the magnetics information consortium (MagIC) database. Geochem. Geophys. Geosyst. 17, 2450–2463. https://doi.org/10.1002/2016GC006307.
Tema, E., Lanos, P., 2021. New Italian directional and intensity archaeomagnetic reference curves for the past 3000 years: Insights on secular variation and implications on dating. Archaeometry 63 (2), 428–445. https://doi.org/10.1111/arcm.12603.
Thellier, E., Thellier, O., 1959. Sur l'intensité du champ magnétique terrestre dans le passé historique et géologique. Ann. Geophys. 15, 285–376.
Ullah, A.K.M., Hossain, A., Akter, M., Kabir, M.F., Khan, M., Fazle Kibria, A.K.M., Firoz, S., 2018. Room temperature ferromagnetic behavior of manganese/manganese oxides nanocomposites. Mater. Lett. 238, 151–154. https://doi.org/10.1016/j.matlet.2018.12.003.
Vernet, E., Carrancho, Á., Calvo-Rathert, M., Arróniz, L., Yamamoto, Y., Bógalo, M.F., Fonseca de la Torre, H.J., 2025. Full vector archaeomagnetic dating of an Early Iron Age archaeological settlement: El Castillar site (Navarra, northern Spain). J. Archaeol. Sci. Rep. 62, 105059. https://doi.org/10.1016/j.jasrep.2025.105059.
Walker, M., 2005. Quaternary Dating Methods. John Wiley & Sons, Ltd. Chichester, England. 304 pp. ISBN: 978-0-470-86927-7.
Yamamoto, Y., Tsunakawa, H., Shibuya, H., 2003. Paleointensity study of the Hawaiian 1960 lava: implications for possible causes of erroneously high intensities. Geophys. J. Int. 153, 263–276. https://doi.org/10.1046/j.1365-246X.2003.01909.x.
Yamamoto, Y., Tsunakawa, H., 2005. Geomagnetic field intensity during the last 5 Myr: LTD-DHT Shaw palaeointensities from volcanic rocks of the Society Islands, French Polynesia. Geophys. J. Int. 162, 79–114. https://doi.org/10.1111/j.1365-246X.2005.02651.x.
Yamamoto, Y., Torii, M., Natsuhara, N., 2015. Archeointensity study on baked clay samples taken from the reconstructed ancient kiln: implication for validity of the Tsunakawa-Shaw paleointensity method. Earth Planets Space 67, 63. https://doi.org/10.1186/s40623-015-0229-8.
Yamamoto, Y., Tauxe, L., Ahn, H., Santos, C., 2022. Absolute paleointensity experiments on aged thermoremanent magnetization: assessment of reliability of the Tsunakawa-Shaw and other methods with implications for "fragile" curvature. Geochem. Geophys. Geosyst. 23, e2022GC010391. https://doi.org/10.1029/2022GC010391.